Virology 454-455 (2014) 263–269

Contents lists available at ScienceDirect

Virology

journal homepage: www.elsevier.com/locate/yviro

Respiratory syncytial virus increases lung cellular bioenergetics in neonatal C57BL/6 mice

Ahmed R. Alsuwaidi [a,*], Alia Albawardi [b], Saeeda Almarzooqi [b], Sheela Benedict [a], Aws R. Othman [a], Stacey M. Hartwig [c], Steven M. Varga [c,**], Abdul-Kader Souid [a]

[a] Departments of Pediatrics, College of Medicine and Health Sciences, United Arab Emirates University, P.O. Box 17666, Al Ain, United Arab Emirates
[b] Departments of Pathology, College of Medicine and Health Sciences, United Arab Emirates University, P.O. Box 17666, Al Ain, United Arab Emirates
[c] Department of Microbiology, Department of Pathology and Interdisciplinary Graduate Program in Immunology, University of Iowa, Iowa City, IA 52242, USA

ARTICLE INFO

Article history:
Received 14 December 2013
Returned to author for revisions
31 January 2014
Accepted 28 February 2014
Available online 21 March 2014

Keywords:
Respiratory syncytial virus
Cellular respiration
Oxygen consumption
Cellular ATP
Mitochondria
Neonates
Mice
C57BL/6

ABSTRACT

We have previously reported that lung cellular bioenergetics (cellular respiration and ATP) increased in 4–10 week-old BALB/c mice infected with respiratory syncytial virus (RSV). This study examined the kinetics and changes in cellular bioenergetics in ≤2-week-old C57BL/6 mice following RSV infection. Mice (5–14 days old) were inoculated intranasally with RSV and the lungs were examined on days 1–10 post-infection. Histopathology and electron microscopy revealed preserved pneumocyte architectures and organelles. Increased lung cellular bioenergetics was noted from days 1–10 post-infection. Cellular GSH remained unchanged. These results indicate that the increased lung cellular respiration (measured by mitochondrial O_2 consumption) and ATP following RSV infection is independent of either age or genetic background of the host.

© 2014 Elsevier Inc. All rights reserved.

Introduction

Cellular bioenergetics including mitochondrial O_2 consumption and ATP synthesis is necessary for viral survival. Viruses commonly alter host cellular processes including gene expression, protein synthesis and membrane structure to facilitate viral replication (Maynard et al., 2010). Abundant nutrients and efficient flux of metabolic fuels are essential to support this process. Poliomyelitis virus, for example, stimulates glycolysis and ATP synthesis (Green et al., 1958; Levy and Baron, 1957). Similarly, human cytomegalovirus promotes glycolysis, citric acid cycle and nucleotide biosynthesis (Munger et al., 2006). Influenza virus infection exerts compound effects on host cell glycolysis (Fisher and Ginsberg, 1956; Klemperer, 1961). Thus, the metabolic impact of a viral infection within a host cell is complex and can vary widely between different viruses.

Cellular bioenergetics includes all metabolic processes involved in energy conversion. Cellular respiration, on the other hand, implies delivery of O_2 and metabolic fuels to the mitochondria, oxidation of reduced metabolic fuels and passage of electrons to O_2 to form H_2O (water of oxidation).

We have previously reported that RSV induces increased cellular respiration and ATP in the lungs of adult BALB/c mice during the first week of infection (Alsuwaidi et al., 2013c). Following clearance of the virus, both cellular respiration rates and ATP levels return to pre-infection levels. In this study, we evaluated lung cellular respiration and ATP in neonatal C57BL/6 mice following RSV infection.

Results

Impact of RSV on lung cellular respiration and ATP in mouse neonates

Fig. 1 shows representative runs of lung cellular mitochondrial O_2 consumption on days 2, 4 and 10 post-infection. O_2 concentration decreased linearly with time. The rate of respiration (k_c in μM

* Corresponding author. Tel.: +971 3 713 7411; fax: +971 3 767 2022.
** Corresponding author. Tel.: +319 335 8433.
E-mail addresses: alsuwaidia@uaeu.ac.ae (A.R. Alsuwaidi), alia.albawardi@uaeu.ac.ae (A. Albawardi), saeeda.almarzooqi@uaeu.ac.ae (S. Almarzooqi), sheela.benedict@uaeu.ac.ae (S. Benedict), aws.rashad@uaeu.ac.ae (A.R. Othman), stacey-hartwig@uiowa.edu (S.M. Hartwig), steven-varga@uiowa.edu (S.M. Varga), asouid@uaeu.ac.ae (A.-K. Souid).

http://dx.doi.org/10.1016/j.virol.2014.02.028
0042-6822 © 2014 Elsevier Inc. All rights reserved.

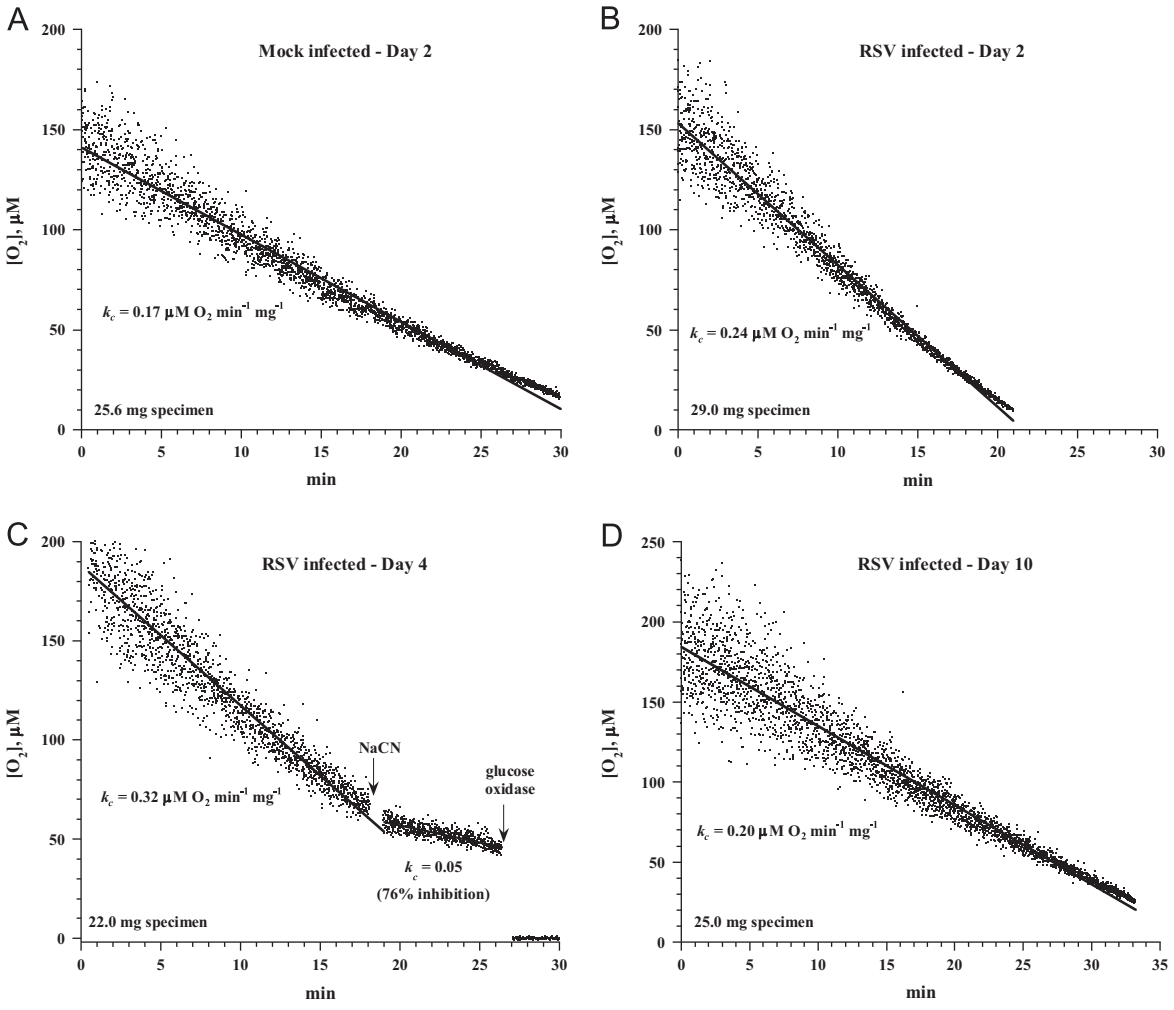

Fig. 1. Lung tissue cellular respiration in RSV infected and mock infected mice. Representative runs of cellular mitochondrial O_2 consumption by lung specimens are shown. The O_2 measurements were performed at 37 °C *immediately* after sample collection. The lung fragments were placed in a sealed glass vial containing Krebs-Henseleit buffer supplemented with 3 µM Pd phosphor and 0.5% fat-free albumin. The rate of respiration (k in µM O_2 min^{-1}) was the negative of slope of [O_2] *vs.* t. The values of k were corrected for sample weight (k_c in µM O_2 min^{-1} mg^{-1}). The additions of 10 mM NaCN and 50 µg/mL glucose oxidase are shown.

O_2 min^{-1} mg^{-1}) in mock infected lungs on day 2 was 0.17 (Fig. 1A); the corresponding rate in the infected lungs was 0.24 representing a 40% increase (Fig. 1B). The values of k_c on days 4 and 10 post-infection were 0.32 (Fig. 1C) and 0.20 (Fig. 1D), respectively. O_2 consumption was inhibited by cyanide (Fig. 1C), confirming this zero-order kinetic process occurred mainly in the mitochondrial respiratory chain. The reversible inhibition of cytochrome c oxidase by cyanide was incomplete, reflecting a known "leak" past the cyanide block (Slater, 1967). The addition of glucose oxidase (catalyzing the reaction: D-glucose + O_2 → D-glucono-δ-lactone + H_2O_2) depleted remaining O_2 in the solution.

Fig. 2A and B shows the kinetics of changes in cellular respiration (panel A) and ATP (panel B) as a function of days post-inoculation with either RSV or PBS in 5–9 day-old-mice. The measured bioenergetic markers were higher from days 1–10 post-infection. For days 1–10, the average (±SD) rate of cellular respiration (k_c in µM O_2 min^{-1} mg^{-1}) in mock infected lungs was 0.119 ± 0.046 ($n=24$) and in infected lungs it was 0.161 ± 0.072 ($n=29$, 35% higher, $p=0.052$), Fig. 2A. Cellular ATP content (pmol mg^{-1}) in mock infected lungs was 184 ± 60 ($n=14$) and in infected lungs it was 294 ± 98 ($n=18$, 75% higher, $p<0.001$), Fig. 2B. Both lung cellular respiration and ATP nearly doubled on day 4 post-infection ($p=0.010$ and $p=0.057$, respectively).

Fig. 2C and D shows the kinetics of changes in cellular respiration (panel C) and ATP (panel D) as a function of days post-inoculation with either RSV or PBS in 13-day-old-mice. Similarly, the bioenergetic markers were also higher from days 2–10 post-infection. For days 2–10, the value of k_c in mock infected lungs was 0.090 ± 0.028 µM O_2 min^{-1} mg^{-1} ($n=11$) and in infected lungs it was 0.167 ± 0.028, representing an 85% increase ($n=15$, $p=0.002$), Fig. 2C. Cellular ATP in mock infected lungs was 175 ± 54 pmol mg^{-1} ($n=9$) and in infected lungs it was 318 ± 178 ($n=12$, 82% higher, $p=0.001$), Fig. 2D. Both lung cellular respiration and ATP content peaked after day 4 post-infection. Therefore, lung cellular respiration and ATP were significantly increased from days 1–10 post-infection in both age groups (≤9-day-old and 13-day-old mice).

In C57BL/6 mice of ≥4 weeks of age, the rate of respiration (k_c in µM O_2 min^{-1} mg^{-1}) in mock infected lungs on days 3–5 post-inoculation was 0.07 ± 0.02 ($n=7$) and in RSV infected mice it was 0.14 ± 0.06 ($n=8$, $p=0.004$).

The augmented cellular respiration in RSV infection is lung-specific. The heart muscle cellular respiration was unaffected by RSV infection (data not shown). For example, on day 7 post-inoculation, the rate of cardiomyocyte respiration in a mock infected mouse was 0.22 µM O_2 min^{-1} mg^{-1} and in a RSV infected mouse it was 0.18 µM O_2 min^{-1} mg^{-1}.

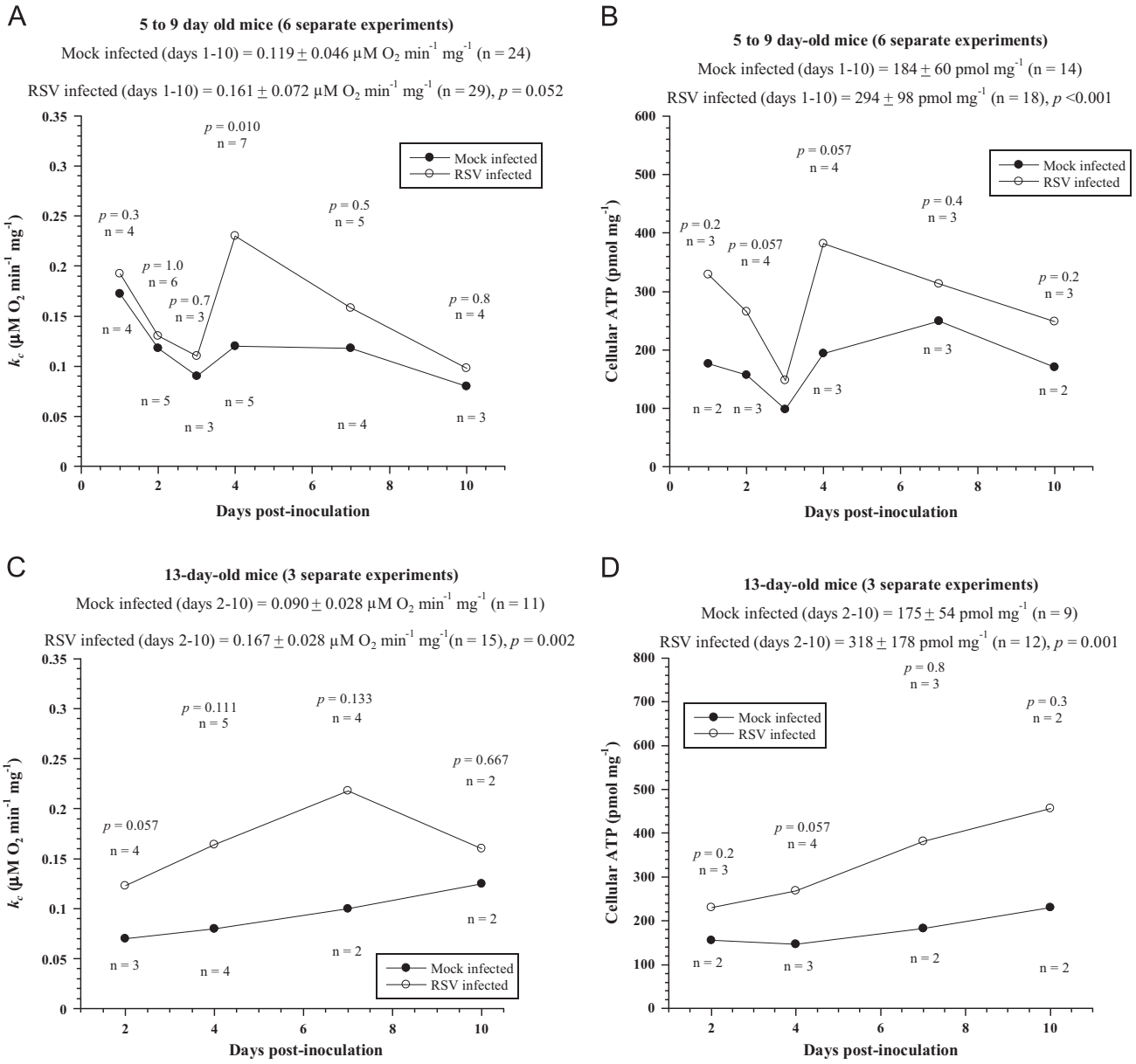

Fig. 2. Lung tissue cellular respiration and ATP in RSV infected and mock infected mice. Rates of cellular respiration (panels A and C) and ATP (panels B and D) as a function of days post-inoculation with the RSV or PBS for 5–9 day old (panels A and B) and 13-day-old mice. Ten experiments (98 mice) included measurements of respiration. Twelve experiments (72 mice) included measurements of cellular ATP.

Impact of RSV on pneumocyte architectures and organelles in mouse neonates

Fig. 3 shows representative histopathology in infected and mock infected lungs. In mock infected lungs, intact alveolar spaces with sparse interstitial mononuclear cells are present and a few pneumocytes with nuclear pyknosis and apoptotic debris were noted (histopathology score=3); caspase-3 count was <1%. In infected lungs on days 2 and 4, an interstitial mononuclear cell infiltrate was prominent with more pneumocytes exhibiting nuclear pyknosis and an increase in apoptotic debris (histopathology scores=8 and 9, respectively); caspase-3 count was 1%. In infected lungs on day 7, the inflammation was milder and the caspase count was <1% (histopathology score=7), Fig. 3. Representative EM images of mock infected and infected lungs on days 2, 4, 7 and 10 after inoculation are shown in Fig. 4. The pneumocyte architectures and organelles were preserved in all studied specimens.

Impact of RSV on lung tissue GSH and IFN-γ protein levels in mouse neonates

Cellular GSH levels were unchanged throughout the course of infection (7 separate experiments involving 17 mice); the GSH level was 976 ± 170 pmol mg^{-1} ($n=6$) in mock infected lungs and 1029 ± 297 ($n=11$) in infected lungs ($p=0.884$). IFN-γ protein level (pg mg^{-1}) increased in the lung tissue on day 4 post-infection (0.374 ± 0.164 *vs.* 0.600 ± 0.360, $n=9$, $p=0.482$, 5 separate experiments involving 38 mice), Fig. 6D.

Lung tissue reverse transcriptase PCR (RT-PCR) in mouse neonates

Fig. 5 shows representative RT-PCR of lung tissue from 14-day-old mock infected and RSV infected C57BL/6 mice. The RSV genome (334 base pair) was evident on days 2, 4 and 7 post-infection and was absent from mock infected lungs.

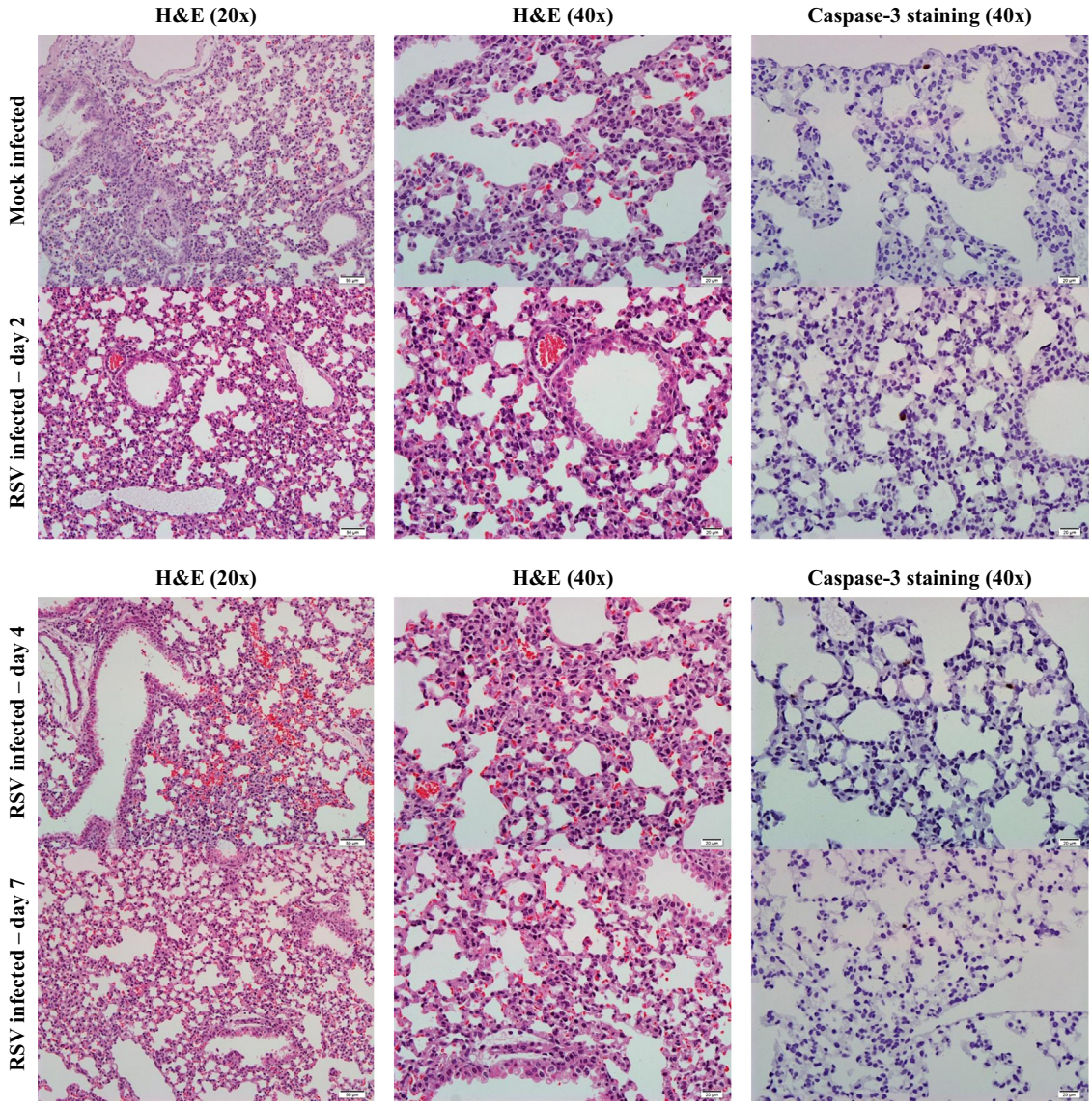

Fig. 3. Lung tissue histopathology (H&E) and caspase-3 staining in RSV infected and mock infected lungs. Note intact alveolar spaces and scant interstitial infiltrates in mock infected lung (histopathology score=3; caspase-3 count $<1\%$). The infiltrate was prominent on days 2 and 4 post-infection with pneumocytes with nuclear pyknosis and apoptotic debris (histopathology scores=8 and 9, respectively; caspase-3 count 1%). The inflammation was milder on day 7 post-infection (histopathology score=7; caspase count $<1\%$). Data are representative of 4 individual experiments with 4–5 mice per experiment.

Discussion

RSV produces a serious infection in human neonates. The underlying mechanisms that mediate the virus-induced pulmonary injury in this age group, however, remain unclear. We have previously reported that lung cellular bioenergetics is enhanced in 4–10 week-old BALB/c mice infected with RSV (Alsuwaidi et al., 2013c). This study investigated lung cellular bioenergetics following acute RSV infection in <2-week-old C57BL/6 mice. Our findings confirm cellular mitochondrial O_2 consumption and ATP are significantly increased in neonates infected with RSV (Fig. 2). Thus, the surrogate biomarkers of lung cellular energy are *not* age or mouse strain specific.

The increased lung cellular bioenergetics correlated with increased interstitial inflammation (Fig. 3), preserved pneumocyte structure and organelles (Fig. 4) and increased IFN-γ protein levels in the lung. It is worth noting that the virus strain (RSV A2), inoculation dose and semi-permissivity of wild-type inbred C57BL/6 mice to human RSV are potential contributors to the observed benign lung histology and low caspase-3 immunostain (Fig. 3).

In contrast to murine lungs infected with influenza A virus (Alsuwaidi et al., 2013a), induction of apoptosis (Figs. 3 and 4) and depletion of cellular GSH are not present in RSV infection. Thus, the RSV infection profile (↑respiration, ↑ATP, ≅apoptosis, ≅GSH; the symbol '≅' indicates congruence) markedly differs from that of influenza A infection (↓respiration, ↓ATP, ↑apoptosis, ↓GSH).

The mechanism by which RSV infection regulates lung cellular respiration is unknown. The virus may accelerate delivery of the reducing equivalents to pneumatocytes, up-regulate critical metabolic enzymes or modulate energy conversion pathways. Further studies are required to verify these potential mechanisms.

The measured biomarkers clearly demonstrate increased energy expenditure in lungs infected with RSV. It is unknown, however, if these changes are induced by the RSV infection or the infiltrating immune cells (Buttgereit et al., 2000). It is worth noting that murine lungs infected with influenza A demonstrate impaired lung cellular bioenergetics despite the prominent inflammation induced by the virus (Alsuwaidi et al., 2013a). It is also unknown whether recovery from either RSV or influenza A infection requires increased pneumocyte bioenergetics.

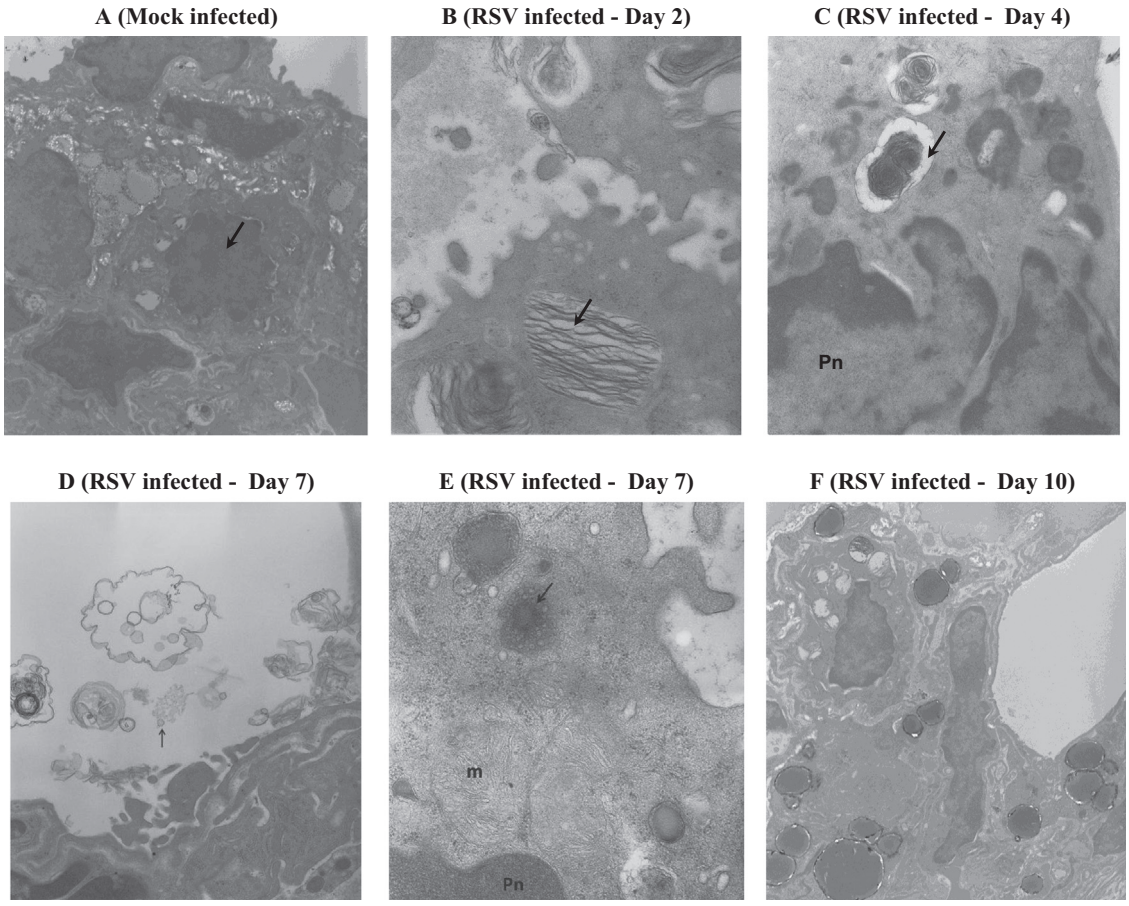

Fig. 4. Electron microscopy (EM) images of RSV infected and mock infected lungs. *Panel A*: mock infected lung showing well-preserved pneumocyte structure (arrow) and cellular organelles (magnification ×4900). *Panel B*: infected lung (Day 2) showing preserved cellular organelles including lamellar bodies (arrow) of type-II pneumocytes (magnification ×27,500). *Panel C*: infected lung (Day 4) showing the cellular organelles being well-preserved. Note the nucleus of type-II pneumocyte (Pn) and lamellar bodies (arrow) (magnification ×18,000). *Panel D*: infected lung (Day 7); the arrow demonstrates pleomorphic round viral particles (arrow) present outside a cell adjacent to filamentaous viral particles just superior to it (magnification ×14,000). *Panel E*: infected lung (Day 7) showing that most cells contained a relatively well-preserved mitochondria; only some had swollen mitochondria (m) as seen in image. Note the cytoplasmic vesicle with viral particles (arrow) (magnification ×275,000). *Panel F*: infected lung (Day 10) showing the cellular details and integrity are preserved (magnification ×4900). Pn—pneumocyte, and m—mitochondria. One experiment (12 mice) was performed.

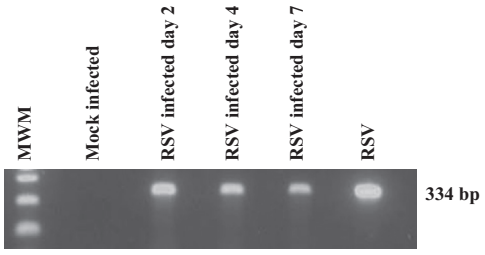

Fig. 5. Reverse transcriptase (RT) PCR of lung tissue from 14-day-old mock infected and RSV infected C57BL/6 mice. Molecular weight markers (MWM): 250, 350 and 450 base pair (bp) were used. The molecular weight of RSV is shown (334 bp). Representative of two separate experiments (10 mice) is shown.

Viral-induced reactive O_2 species (ROS) are known to deplete cellular GSH depletion and induce apoptosis (Snelgrove et al., 2006). The findings that GSH and caspase levels remain unchanged suggest a minimum role for ROS in RSV infection. Influenza A virus, on the other hand, is associated with GSH depletion (ROS production) and induction of apoptosis (Alsuwaidi et al., 2013a; Snelgrove et al., 2006).

The impact of changes in lung cellular bioenergetics on the understanding of RSV infection requires further investigation. Intact mitochondria and lack of caspase activities are required to support increased cellular energy demand (expenditure) in the lungs following acute RSV infection. Adequate nutrition of infants infected with RSV is essential to meet these increased metabolic requirements. The increased nutrient demand cannot be fully met during influenza A virus infection due to mitochondrial dysfunction as indicated by inhibition of cellular respiration and decreased of cellular ATP (Alsuwaidi et al., 2013a).

In conclusion, intact mitochondrial function (pneumocyte bioenergetics) and structure are hallmarks of RSV infected lungs, supporting the increased energy demand set by the virus or associated inflammation.

Materials and methods

Reagents and solutions

Pd(II) complex of *meso*-tetra-(4-sulfonatophenyl)-tetrabenzoporphyrin (Pd phosphor) was purchased from Porphyrin Products (Logan, UT). Monobromobimane (mBBr, 271.111) was purchased from Molecular Probes (Eugene, Oregon). Complete® protease inhibitor cocktail was purchased from Roche Applied Science (Indianapolis, IN). Avidin-biotin immunoperoxidase was purchased from Cell Signaling Technology (Boston, MA). Glucose, GSH (mol. wt. 307.43), HPLC-grade methanol, trifluoroacetic acid,

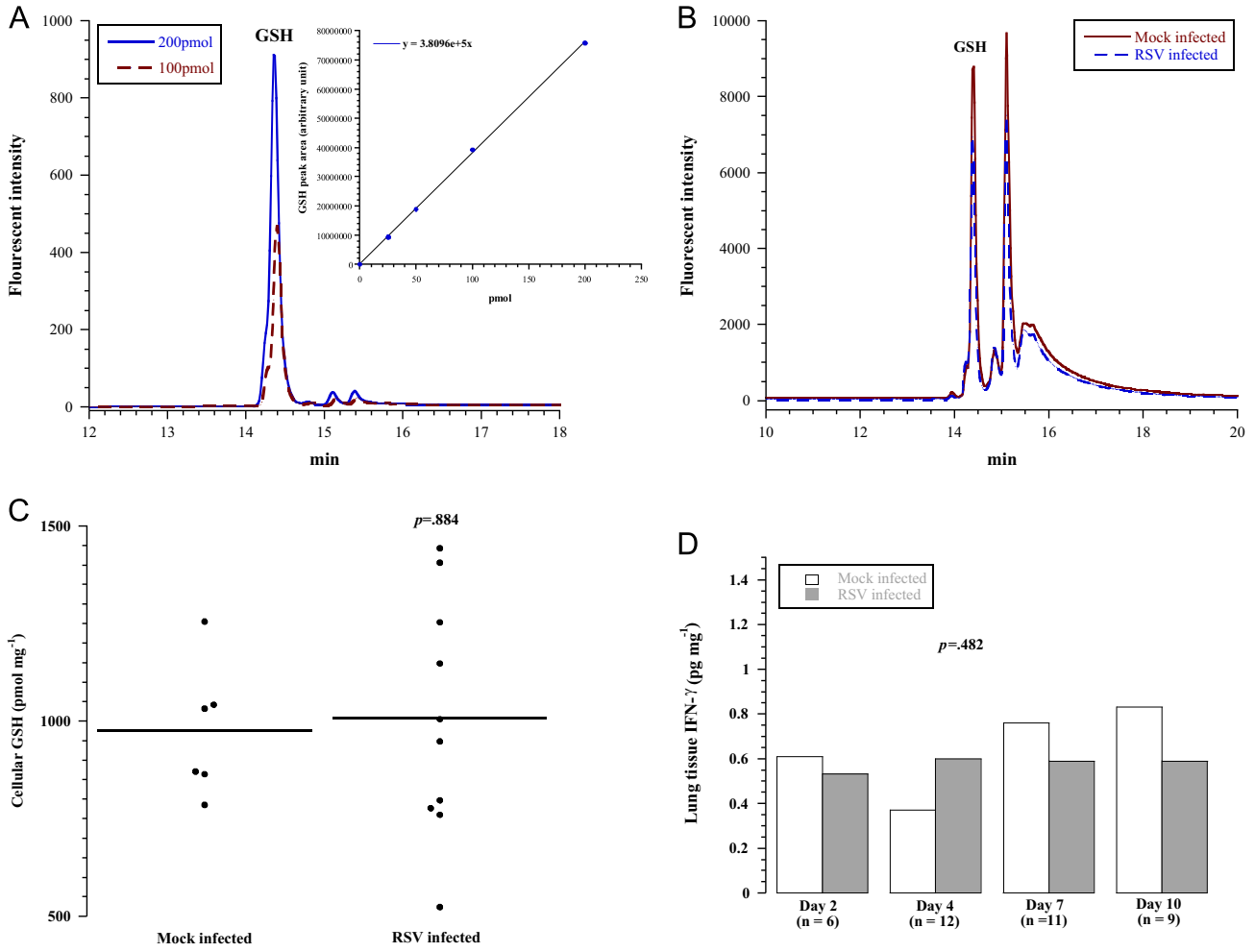

Fig. 6. Lung tissue GSH and IFN-γ. *Panel A*: representative HPLC runs of 100 and 200 pmol GSH (retention time = ~14.2 min). *Panel B*: representative HPLC runs of cellular GSH in mock infected and RSV infected lungs. *Panel C*: summary results of GSH (7 separate experiments involving 17 mice). *Panel D*: lung tissue IFN-γ protein levels.

N-ethylmaleimide (NEM, forms thioether bonds with sulfhydryls) and remaining reagents were purchased from Sigma-Aldrich (St. Louis, MO).

Pd phosphor, NaCN, GSH, glucose oxidase and Krebs-Henseleit buffer were prepared as described (Alsuwaidi et al., 2013b, 2013c; Jocelyn, 1987; Souid et al., 2001). NEM (0.1 M) was made in ethanol and stored at −20 °C. One tablet of the Complete® protease inhibitors was dissolved in 2.0 mL dH_2O and stored at −20 °C. For O_2 measurement, the lung specimens were *immediately* placed in 1 mL glass vials containing 1.0 mL Krebs-Henseleit buffer with 3 μM Pd phosphor and 0.5% albumin. The vials were sealed from air and O_2 concentrations were determined at 37 °C as a function of time as described (Alsuwaidi et al., 2013b). Specimens were *immediately* processed for ATP, IFN-γ, and PCR as previously described (Alsuwaidi et al., 2013b, 2013c). GSH was labeled with mBBr and analyzed on HPLC as described (Souid et al., 2001).

RSV infection

RSV A2 was propagated in HEp-2 cells as previously described (Alsuwaidi et al., 2013c). C57BL/6 mice, 5–14 days old, (Jackson Laboratory, Bar Harbor, ME) were housed in a room maintained at 22 °C with 60% relative humidity. All protocols received approval from the Animal Ethics Committee—UAE University—College of Medicine and Health Sciences (Protocol no. A12/11). Mice were inoculated intranasally with 4.8×10^5 pfu, equivalent to approximately $0.5–1.0 \times 10^5$ pfu per gram body weight, in 15 μl total volume of either RSV A2 or phosphate buffered saline (PBS). Mice were grouped into RSV infected and mock infected and remained with their mothers in separate cages. The mice were anesthetized by sevoflurane inhalation (100 μl per 10 g) and sacrificed on days 1–10 following infection (Alsuwaidi et al., 2013b). Sixteen separate experiments involving 147 mice were performed.

Histology

Specimens were *immediately* processed for histology as previously described (Alsuwaidi et al., 2013b, 2013c). Each section was graded based on the following categories: (A) peribronchiolar and bronchial infiltrates (none, < 25%, 25–75%, and > 75%); (B) quality of peribronchiolar and bronchial infiltrates (none, interrupted collar, complete collar < 5 cells thick, and complete collar > 5 cells thick); (C) bronchiolar and bronchial luminal exudates (none, ≤ 25% luminal occlusion, and ≥ 25% luminal occlusion); (D) perivascular infiltrates (none, < 10%, 10–50%, and > 50%), and (E) parenchymal pneumonia (none, patchy parenchymal infiltrates, and heavy parenchymal infiltrates). A numeric score that ranged from 0 to 26 was calculated as: "A + 3(B + C) + D + E" (Cimolai et al., 1992; Hardy et al., 2001).

Staining for apoptosis was performed using avidin-biotin immunoperoxidase, which detected active caspase-3. The procedure was performed on 3 μm paraffin sections using rabbit

anti-cleaved caspase-3 (Alsuwaidi et al., 2013b). Samples were also processed for electron microscopy (EM) as previously described (McDowell and Trump, 1976).

IFN-γ

The mouse cytokine ELISA kit (E-Biosciences, San Diego, CA) was used to detect IFN-γ. Lung specimens were homogenized in 1.0 mL of KH buffer supplemented with 40 μl Complete® protease inhibitors. The supernatants were collected by centrifugation ($1000 \times g$ at 4 °C for 20 min) and assayed in duplicate. The standard curve (15–2000 pg/ml) was linear ($R > 0.99$) and the detection sensitivity was 15 pg/ml.

Statistical analysis

The nonparametric test (2 independent variables) of Mann-Whitney was used (SPSS statistical package, version 19).

Acknowledgments

This research is supported by a grant from the United Arab Emirates University (31M117).

References

Alsuwaidi, A.R., Almarzooqi, S., Albawardi, A., Benedict, S., Kochiyil, J., Mustafa, F., Hartwig, S.M., Varga, S.M., Souid, A.K., 2013a. Cellular bioenergetics, caspase activity and glutathione in murine lungs infected with influenza A virus. Virology 446, 180–188.

Alsuwaidi, A.R., Alsamri, M.T., Alfazari, A.S., Almarzooqi, S., Albawardi, A., Othman, A.R., Pramathan, T., Hartwig, S.M., Varga, S.M., Souid, A.K., 2013b. Lung tissue bioenergetics and caspase activity in rodents. BMC Res. Notes 6, 12.

Alsuwaidi, A.R., Benedict, S., Kochiyil, J., Mustafa, F., Hartwig, S.M., Almarzooqi, S., Albawardi, A., Rizvi, T.A., Varga, S.M., Souid, A.K., 2013c. Bioenergetics of murine lungs infected with respiratory syncytial virus. Virol. J. 10, 22.

Buttgereit, F., Burmester, G.R., Brand, M.D., 2000. Bioenergetics of immune functions: fundamental and therapeutic aspects. Immunol. Today 21, 192–199.

Cimolai, N., Taylor, G.P., Mah, D., Morrison, B.J., 1992. Definition and application of a histopathological scoring scheme for an animal model of acute *Mycoplasma pneumoniae* pulmonary infection. Microbiol. Immunol. 36, 465–478.

Fisher, T.N., Ginsberg, H.S., 1956. The reaction of influenza viruses with guinea pig polymorphonuclear leucocytes. II. The reduction of white blood cell glycolysis by influenza viruses and receptor-destroying enzyme (RDE). Virology 2, 637–655.

Green, M., Henle, G., Deinhardt, F., 1958. Respiration and glycolysis of human cells grown in tissue culture. Virology 5, 206–219.

Hardy, R.D., Jafri, H.S., Olsen, K., Wordemann, M., Hatfield, J., Rogers, B.B., Patel, P., Duffy, L., Cassell, G., McCracken, G.H., Ramilo, O., 2001. Elevated cytokine and chemokine levels and prolonged pulmonary airflow resistance in a murine *Mycoplasma pneumoniae* pneumonia model: a microbiologic, histologic, immunologic, and respiratory plethysmographic profile. Infect. Immun. 69, 3869–3876.

Jocelyn, P.C., 1987. Spectrophotometric assay of thiols. Methods Enzymol. 143, 44–67.

Klemperer, H., 1961. Glucose breakdown in chick embryo cells infected with influenza virus. Virology 13, 68–77.

Levy, H.B., Baron, S., 1957. The effect of animal viruses on host cell metabolism. II. Effect of poliomyelitis virus on glycolysis and uptake of glycine by monkey kidney tissue cultures. J. Infect. Dis.100, 109–118.

Maynard, N.D., Gutschow, M.V., Birch, E.W., Covert, M.W., 2010. The virus as metabolic engineer. Biotechnol. J. 5, 686–694.

McDowell, E.M., Trump, B.F., 1976. Histologic fixatives suitable for diagnostic light and electron microscopy. Arch. Pathol. Lab. Med. 100, 405–414.

Munger, J., Bajad, S.U., Coller, H.A., Shenk, T., Rabinowitz, J.D., 2006. Dynamics of the cellular metabolome during human cytomegalovirus infection. PLoS Pathog. 2, e132.

Slater, E.C., 1967. Application of inhibitors and uncouplers for a study of oxidative phosphorylation. In: Estabrook, R.W., Pullman, M.E. (Eds.), Method Enzymol., 10. Academic Press, New York and London, pp. 48–57.

Snelgrove, R.J., Edwards, L., Rae, A.J., Hussell, T., 2006. An absence of reactive oxygen species improves the resolution of lung influenza infection. Eur. J. Immunol. 36, 1364–1373.

Souid, A.K., Fahey, R.C., Aktas, M.K., Sayin, O.A., Karjoo, S., Newton, G.L., Sadowitz, P. D., Dubowy, R.L., Bernstein, M.L., 2001. Blood thiols following amifostine and mesna infusions, a pediatric oncology group study. Drug Metab. Dispos.: Biol. Fate Chem. 29, 1460–1466.